ACS APPLIED MATERIALS & INTERFACES

Research Article

www.acsami.org

Fe-Based Metallopolymer Nanowall-Based Composites for Li–O_2 Battery Cathode

Wenyu Zhang,[†,‡] Jixin Zhu,[†,‡] Huixiang Ang,[†] Haibo Wang,[∥] Hui Teng Tan,[†,‡] Dan Yang,[†,‡] Chen Xu,[†,‡] Ni Xiao,[†] Bing Li,[⊥] Weiling Liu,[†] Xin Wang,[∥] Huey Hoon Hng,[†] and Qingyu Yan*[,†,‡,§]

[†]School of Materials Science and Engineering, Nanyang Technological University, Singapore, 639798, Singapore

[‡]TUM CREATE Research Centre@NTU, Nanyang Technological University, Singapore 637459, Singapore

[§]Energy Research Institute@NTU, Nanyang Technological University, Singapore 637553, Singapore

[∥]School of Chemical and Biomedical Engineering, Nanyang Technological University, Singapore 637459, Singapore

[⊥]Institute of Materials Research and Engineering, Singapore 117602, Singapore

Supporting Information

ABSTRACT: Metallopolymer nanowalls were prepared through a simple wet-chemical process using reduced graphene oxides as heterogeneous nucleation aids, which also help to form conductive electron paths. The nanowalls grow vertically on graphene surface with 100 -200 nm in widths and ~20 nm in thickness. The Fe-based metallopolymer nanowall-based electrode shows best performance as O_2 cathode exhibiting high round-trip efficiencies and stable cycling performance among other transition metal containing metallopolymer counterparts. The electrode delivers discharge–charge capacities of 1000 mAh/g for 40 cycles and maintains round-trip efficiencies >78 % at 50 mA/g. The 1st-cycle round-trip efficiencies are 79%, 72%, and 65% at current densities of 50, 200, and 400 mA/g, respectively. The NMR analysis of the Fe-based metallopolymer based electrode after 40 cycles reveals slow formation of the side products, CH_3CO_2Li and HCO_2Li.

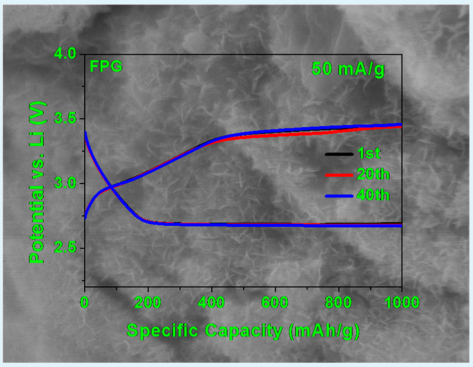

KEYWORDS: *Li–O_2 battery, O_2 electrodes, metal-organic frameworks*

1. INTRODUCTION

Advances in rechargeable Li-ion batteries deliver on the promise of cycle life, safety, and mobility, making them gaining wide acceptance as an ideal energy solution.[1] Great efforts have been devoted to further improving their electrochemical performances. In recent years, new types of Li-based energy systems, especially the Li–O_2 batteries (LOBs) has moved to the frontline to meet the increasing-demand in the area of electric vehicles and portable devices due to their exceptionally high theoretical energy densities.[2−16] However, LOBs suffers from the sluggish kinetics of the oxygen reduction reaction (ORR) and the oxygen evolution reaction (OER) on O_2 electrodes during cycling. Other requirements of O_2 electrodes include high specific surface area, high electrical conductivity and high electrochemical stability, which are beneficial to achieve excellent energy storage properties of LOBs.

To improve the ORR and OER kinetics, great efforts have been devoted to exploring efficient electrocatalysts in pursuit of technological breakthrough. In this regard, precious metals, rare earth elements based materials and transition metal oxides have been intensively investigated but their practical applications are limited by prohibitively high cost, tedious synthesis procedures and toxicity of the heavy metal-containing compounds.[5,17−19] Alternatively, the metallopolymers that possess metal-N sites emerged as a new class of efficient electrocatalysts by exploiting the coordination chemistry between nitrogen atom of pyrrole units and the transition metal atoms to form the metal-N bonds.[20−23] Such architectures endow them with excellent catalytic activities towards the oxygen related reactions in comparison to the precious metals, making them promising candidates for LOBs application.

In this work, the metallopolymers were synthesized as the electrocatalysts for LOBs. To enhance the electrical conductivity of the O_2 electrodes, reduced graphene oxide[24−30] was incorporated as the conductive scaffold of the metallopolymers. The metallopolymers nanowall arrays with thickness of ~20 nm were grown vertically on the graphene sheets. This unique morphology is beneficial for efficient O_2 diffusion in LOBs[18,31,32] and to prevent graphene from restacking. Among all of the as-synthesized samples, the Fe-based metallopolymer composite exhibited better catalytic efficiency and excellent electrochemical stabilities for LOBs, e.g. delivering discharge/charge capacities of 1000 mAh/g for 40 cycles with energy efficiency (round-trip efficiency) of >78 %.

Received: January 10, 2014
Accepted: April 24, 2014
Published: April 24, 2014

 © 2014 American Chemical Society

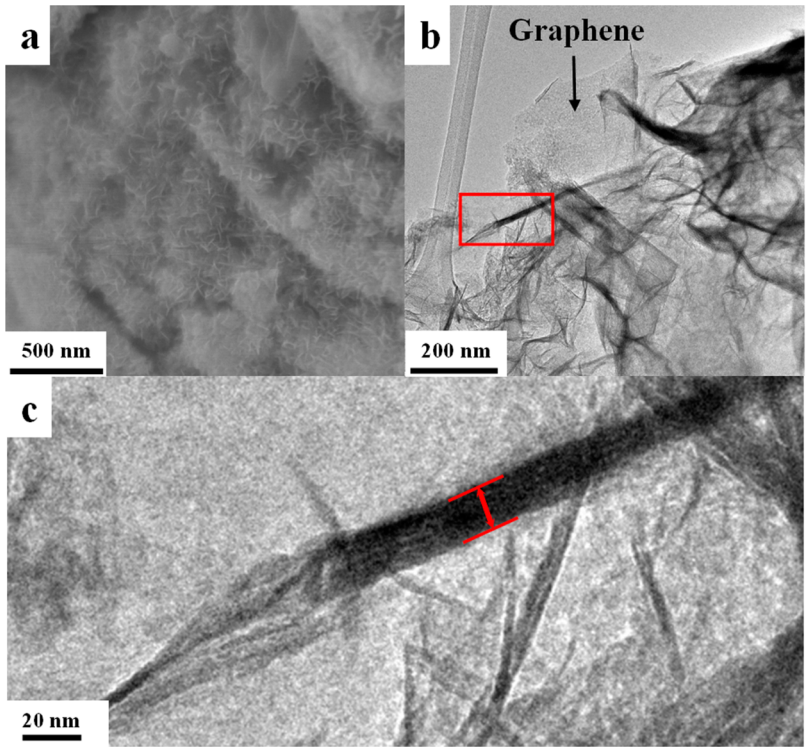

Figure 1. (a) SEM image, (b, c) TEM images of Fe-based metallopolymer/reduced graphene oxide. Image c is the magnified area of the red square in b.

2. EXPERIMENTAL SECTION

2.1. Synthesis of Reduced Graphene Oxide (rGO). Graphite oxide was prepared by a modified Hummer's method.[33−35] The aqueous solution of concentrated H_2SO_4 (12 g), $K_2S_2O_8$ (2.5 g), and P_2O_5 (2.5 g) was heated to 80°C, followed by the addition of graphite powder (3 g). The mixture was kept at 80°C for 4.5 h. The preoxidized product was washed with deionized water and dried in a vacuum oven for overnight. The graphite powder was then added into concentrated H_2SO_4 (120 mL) in an ice bath, followed by slow addition of $KMnO_4$ (15 g). After the mixture was kept at 35°C for 2 h, de-ionized water (250 mL) was put into the mixture and stirred for 2 h. Then de-ionized water (0.7 L) and 30 % H_2O_2 (20 mL) was added. The mixture was washed with diluted HCl aqueous solution and de-ionized water. The product (graphite oxide) was dried in vacuum oven for overnight.

The graphite oxide (100 mg) was dispersed in de-ionized water (100 mL) and sonicated for 1 h. An aqueous solution of cetrimonium bromide (4 mL, 0.5 wt %) and $NaBH_4$ (2 g) was added and kept at 100°C for 4 h. The final product was washed dried in vacuum oven.

2.2. Synthesis of Polypyrrole/rGO. An aqueous solution of rGO (100 mL, 1 mg/mL) was prepared and mixed with pyrrole (20 mg). 10 % H_2O_2 (100 μL) was added into the solution and stirred at room temperature for 3 h. Then the product was washed with de-ionized water and dried in vacuum.

2.3. Synthesis of Fe-Based Metallopolymer/rGO (FMG). The polypyrrole/rGO composite (45 mg) was mixed with de-ionized water (10 mL) and heated under reflux for 30 min. $Fe(NO_3)_3$ (24.7 mg in 250μL de-ionized water) was added into the solution and kept at 80°C for 30 min, followed by the addition of the aqueous solution (12.5 mL) of $NaBH_4$ (130 mg) and NaOH (9.2 mg), which was heated to 80°C beforehand. Then the mixture was kept at 80 °C for 30 min. The product was washed and dried in vacuum. The amount of Fe in the composite can be calculated to be ~8.2 wt % by the weight of the composite. Besides, the contents of polypyrrole and reduced graphene oxide are calculated to be ~15.3 and ~76.5 wt %, respectively.

In the synthesis of Co-based metallopolymer/rGO (CMG) and Mn-based metallopolymer/rGO(MMG), $Co(NO_3)_2$, and $Mn(NO_3)_2$ (24.7 mg in 250μL of deionized water) were used to replace $Fe(NO_3)_3$, respectively.

2.4. Materials Characterization. The morphological information on the samples was collected using field-emission scanning electron microscopy (FESEM) (JEOL, model JSM-7600F) and transmission electron microscopy (TEM) (JEOL, Model JEM 2100). The crystal information was examined on powder X-ray diffraction (XRD) (Shimadzu XRD-6000 X-ray diffractometer with Cu Kα irradiation with λ = 1.5406 Å). Raman spectroscopy was performed on WITec CRM 200 with 488 nm wavelength and the spot size was 0.5 mm. The nuclear magnetic resonance (NMR) analysis was carried out on a Bruker 300 NMR spectrometer.

2.5. Electrochemical Characterization. For oxygen reduction reaction tests, Pt foil and HgO/Hg (6M KOH) were used as counter and reference electrode. A glassy carbon electrode with 5 mm diameter was used as the working electrode. The sample was prepared by mixing catalyst dispersion with 0.05 wt % Nafion solution, and dropping the mixture to the glassy carbon electrode.

For Li−O_2 battery tests, the electrodes slurry was prepared by mixing the samples (90 wt %) and poly(vinylidene fluoride) (10 wt %) in *N*-methyl-2-pyrrolidone. After stirring for 1 day, the slurry was coated onto microfiber filter paper (Whatman GF/D) and dried in a vacuum oven for overnight. In a typical LOB cell, Li metal foil was used as the counter and reference electrode. A microfiber filter paper (Whatman GF/D) was applied as the separator and 1 M $LiCF_3SO_3$ in tetra(ethylene) glycol dimethyl ether (TEGDME) as the electrolytes. The construction of the Li−O_2 cells is the same as a previous work.[12] The electrochemical properties of the samples were studied using NEWARE system. All discharge/charge capacities are calculated on the total weight of the composites.

3. RESULTS AND DISCUSSION

The schematic representation of metallopolymer structure shows the linkage between the transition metal atoms and the nitrogen atoms in pyrrole units (see the Supporting Information, Figure S1).[22] Prior to the microscopy characterization, the transmission electron microscope (TEM) electron

beam radiation is used to exam the exact location of the metallopolymers (see the Supporting Information, Figure S2a, b). It demonstrates that the poor stability of the metallopolymers induce their transformation from the nanowalls to the nanoparticles after the high energy radiation.[36] The scanning electron microscope (SEM) image (Figure 1a) and the TEM image (Figure 1b) show that the Fe-based metallopolymer nanowalls with 100−200 nm widths grow vertically on the graphene surface. The high-magnification TEM image (Figure 1c) reveals that the thickness of the Fe-based metallopolymer nanowalls is ∼20 nm. The crystal information on the composites is examined by X-ray diffraction patterns (see the Supporting Information, Figure S3). The peaks at ∼26 and ∼43° can be indexed to the (002) and (100) crystal planes of graphene, respectively. No peaks corresponding to crystalline impurities are detected.

To study the metal-N sites with different metal species, Co-based metallopolymer/rGO (CMG) and Mn-based metallopolymer/rGO (MMG) are also prepared. The SEM images (see the Supporting Information, Figure S4a, b) show that Co-based and Mn-based metallopolymer nanowalls with widths of 200−300 nm are vertically attached on graphene. Similar morphology of FMG, CMG, and MMG hints the growth of metallopolymers is independent of the metal species.

From the Raman spectra shown in Figure 2, typical peaks corresponding to the D and G band of graphene-based

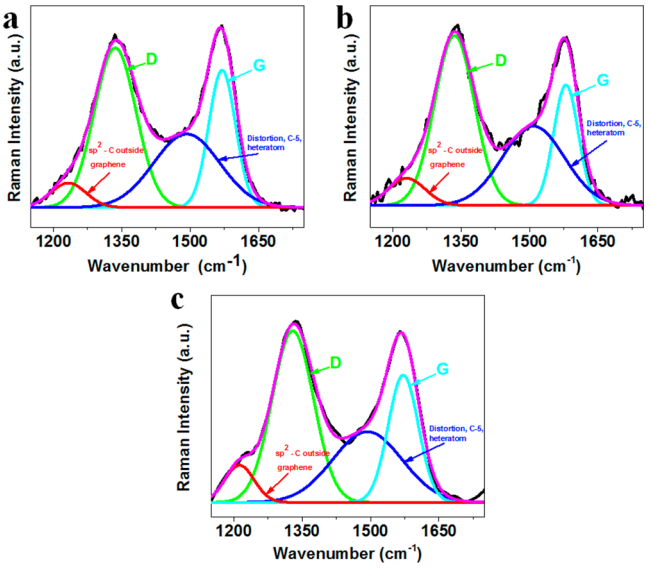

Figure 2. Raman spectra of (a) graphene oxide, (b) reduced graphene oxide, and (c) Fe-based metallopolymer/reduced graphene oxide.

materials appear at around 1365 and 1580 cm^{-1}, respectively for graphene oxide (GO), rGO, and FMG. Typically, two broad peaks at ∼1200 and ∼1510 cm^{-1} are associated with the integrated five-member rings or heteroatoms in the graphene structures.[21] The intensities of these two broad peaks at ∼1200 and ∼1510 cm^{-1} are increased for FMG. This characteristic is manifested in the Raman spectrum of FMG, indicating the successful incorporation of the metallopolymers into the graphene structures. Besides, according to the previous studies, the intensity ratios of the D band and the G band, I_D/I_G, reflects the defect level of graphene-based materials.[37] Here, the I_D/I_G values for GO, rGO and FMG are 1.0, 1.1 and 1.1, respectively, in which the reduction of process has imposed higher defect level in rGO and FMG as compared to GO. The I_D/I_G of rGO and FMG is slightly higher than that of GO because of the reduction process.[35] The X-ray photoelectron spectroscopy (XPS) is performed to investigate the valence state of the major elements in FMG (Figure 3a and b). Peaks of the Fe $2p_{3/2}$ and Fe $2p_{1/2}$ locates at 711.5 and 724.8 eV, respectively, with a satellite peak at ∼719.3 eV, indicating the presence of Fe^{2+}.[33] Fe^{3+} is also detected in the FMG composite as evidenced by the peaks of the Fe $2p_{3/2}$ at 713.6 eV and the Fe $2p_{1/2}$ at 727.4 eV, respectively.[38] It is consistent with the previous study which shows that Fe^{2+} and Fe^{3+} normally coexist in such composite.[22] The presence of N is confirmed by XPS, in which the peak at 400.1 eV in the N 1s spectra corresponds to the pyrrolic N (Figure 3b).[39] On the other hand, the Fe-based metallopolymer without rGO is also prepared and examined (see the Supporting Information, Figure S5a and b). The X-ray diffraction patterns of Fe-based metallopolymer show no peaks. The XPS results confirm the presence of Fe^{2+} and Fe^{3+}, which is similar to FMG. The BET analysis (see the Supporting Information, Figure S6) indicates the specific surface area of FMG is ∼131 m^2 g^{-1} and the average pore diameters of FMG is ∼2.3 nm.

Prior to the LOB test, the catalytic activities of CMG, MMG and FMG are examined by rotating-disk setup (see the Supporting Information, Figure S7). The onset potential of the FMG electrode (∼0.04 V vs. HgO/Hg) is higher than the CMG (∼ -0.08 V vs. HgO/Hg) and the MMG (∼ −0.06 V vs. HgO/Hg), indicating the stronger catalytic activity of the FMG. Furthermore, the electrochemical performance of the FMG composites is investigated in LOBs at various current densities (Figure 4). In a typical discharge process of LOBs, O_2 is reduced and reacts with Li ions to form Li_2O_2 at a standard potential of ∼3 V (vs. Li), which is then reversibly oxidized and releases O_2 during the charge process with high overpotentials (above 4 V vs. Li). It is noticed that the open circuit voltage (OCV) of Li−O_2 cells is higher than the theoretical values (∼3 V), reflecting a mixed potential effect due to the interaction between Li ions in the electrolytes and O_2. The underlying reason for significant increase in the electrochemical potential as well as the OCV could be attributed to the enhanced activity of O_2 in the presence of catalysts. The OCV reflects a mixed potential effect due to the interaction between Li ions in the electrolytes and O_2.[4] The activity of O_2 is enhanced by the catalysts in the electrodes and so the actual electrochemical potential of the electrodes is increased as well as the OCV.[7,40] The round-trip efficiencies, defined as the ratio between the discharge energy and the charge energy, are introduced to evaluate the catalytic effect of the electrodes. The specific discharge−charge capacities of the samples are limited to 1000 mAh/g. The 1st-cycle round-trip efficiencies of the FMG electrodes at current densities of 50, 200, and 400 mA/g are 79, 72, and 65%, respectively. In comparison, the first=cycle round-trip efficiencies of the CMG and MMG electrodes (see the Supporting Information, Figure S8) at 200 mA/g are 67 and 65%, respectively. Therefore, it is concluded that FMG exhibits higher catalytic activities than CMG and MMG. In addition, the round-trip efficiencies of the FMG electrodes are also higher than some of the reported oxygen cathodes, including mesoporous $NiCo_2O_4$ nanoflakes,[41] porous $La_{0.75}Sr_{0.25}MnO_3$ nanotubes,[18] and $CoMn_2O_4$ nanoparticles.[42] On the other hand, the FMG electrodes deliver discharge voltages of ∼2.7 V and charge voltages of ∼3.5 V for 40 cycles at 50 mA/g (Figure 4a). The low charge voltages of the FMG are beneficial to

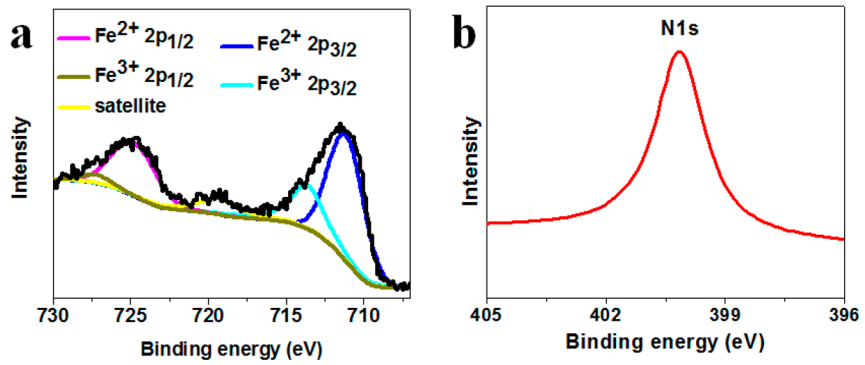

Figure 3. X-ray photoelectron spectra of the Fe-based metallopolymer/reduced graphene oxide: (a) Fe 2p and (b) N 1s spectra.

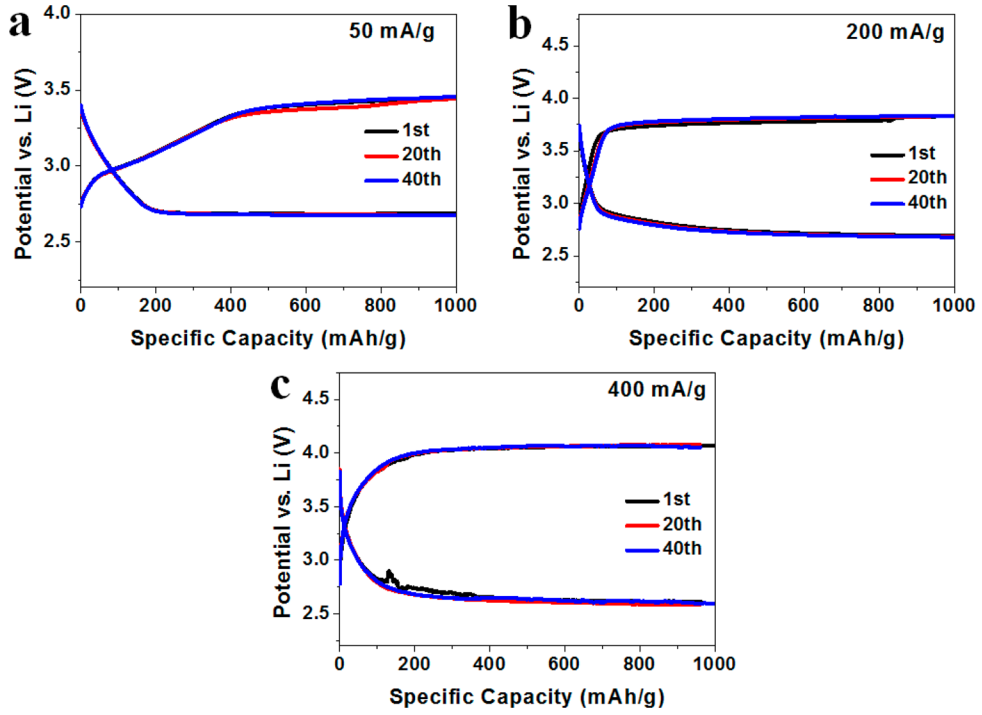

Figure 4. Electrochemical performance of Fe-based metallopolymer/reduced graphene oxide electrodes for Li–O_2 batteries at (a) 50, (b) 200, and (c) 400 mA/g.

suppress the formation of the side products.[43] Moreover, after 40 cycles, the discharge voltages at 200 mA/g are ~2.65 V and the charge voltages are ~3.8 V with a round-trip efficiency of 72 % (Figure 4b), whereas the values at 400 mA/g are ~2.6 V, ~4.1 V, and 65%, respectively (Figure 4c). Such a stable cycling performance under high current densities reveals the superior cathode performance of the FMG electrodes.

To investigate the products after the charge–discharge process, we performed nuclear magnetic resonance (NMR) analysis on the electrodes after 40 cycles (Figure 5). The peaks at 3.3 and 3.6 ppm are generated by TEGDME and the peak at 4.7 ppm corresponds to D_2O. The peaks at 1.8 and 8.3 ppm reveal the presence of CH_3CO_2Li and HCO_2Li, respectively.[44] These two compounds are the side products formed during the cycling process, which can decrease the electrical conductivity and impair the electrochemical properties of the O_2 electrodes. To study the side products quantitatively, equal amounts of D_2O and electrode material of different samples are used in the NMR test. The intensity ratios between the side products and the D_2O ($I_{CH3CO2Li+HCO2Li}/I_{D2O}$) are compared to estimate the contents of the side products generated on the electrodes. The values of $I_{CH3CO2Li+HCO2Li}/I_{D2O}$ are 0.005, 0.003, and 0.001 for the CMG, the MMG and the FMG electrodes, respectively. Therefore, the FGM shows the slowest formation rate of the side products.

The morphologies of the discharged products are also examined. The electrodes discharged to 1000 mAh/g are washed with TEGDME and are handled with care to avoid prolonged exposure to the air. The discharged CMG and MMG show thick and smooth coating layer on the surface of the electrodes (see the Supporting Information, Figure S9a, b). In comparison, the surface of the discharged FMG electrode is rough with numerous bumps (see the Supporting Information, Figure S9c). The formation of the bumps on top of the Fe-based metallopolymer nanowalls may be due to the high catalytic activity of FMG, which induces faster growth of the discharge products near the Fe-based metallopolymer nanowalls (see the Supporting Information, Figure S10a). On the contrary, the growth rates of the discharge products near or far away from the Co-based metallopolymer and Mn-based

dx.doi.org/10.1021/am500158s | ACS Appl. Mater. Interfaces 2014, 6, 7164–7170

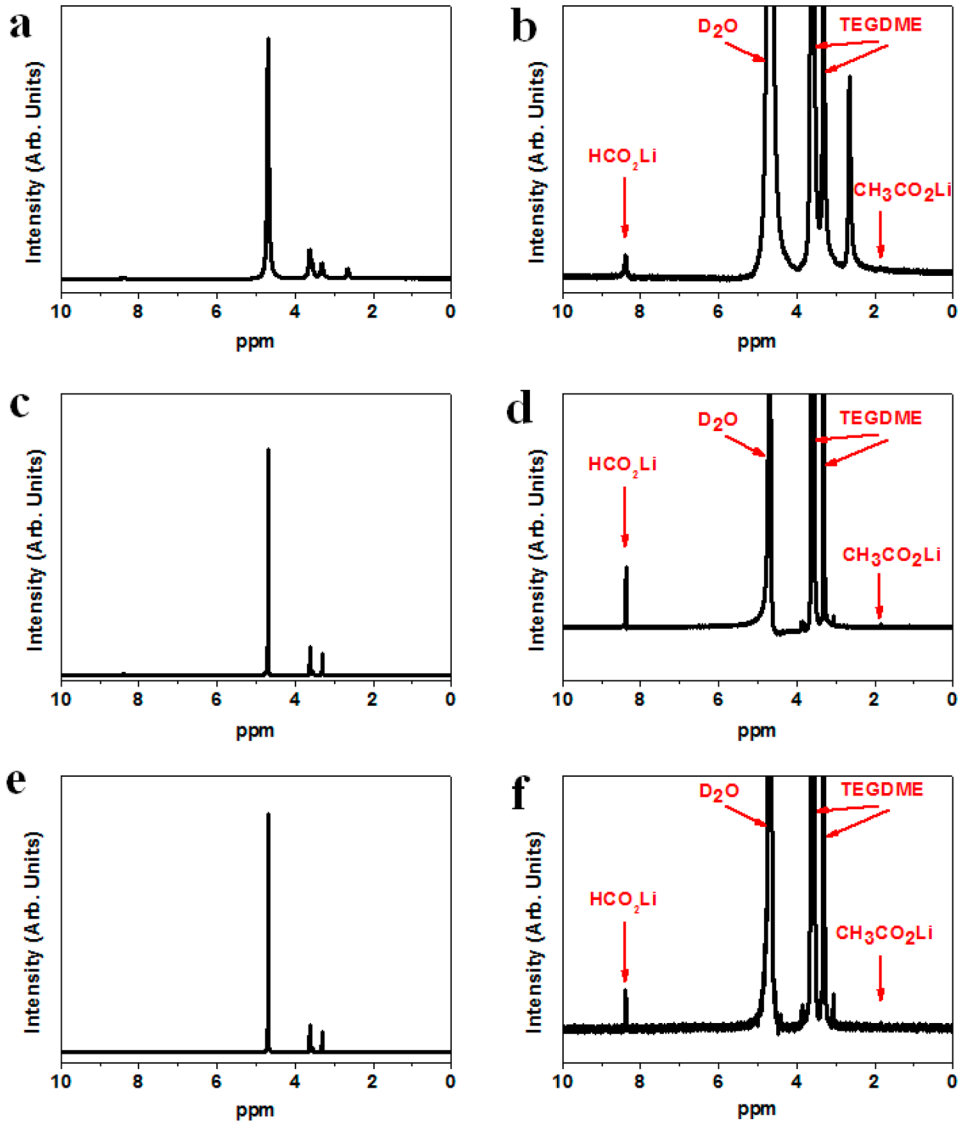

Figure 5. ^{1}H NMR spectra of (a, b) Co-based metallopolymer/rGO, (c, d) Mn-based metallopolymer/rGO, and (e, f) Fe-based metallopolymer/rGO after 40 cycles. b, d, and f are the magnified spectra.

metallopolymer nanowalls do not show much difference because of their moderate catalytic activities (see the Supporting Information, Figure S10b). Hence no obvious bumps are formed on the surface of CMG and MMG. Besides, the rough surface of the discharge products on the FMG electrode increases the contact area of the discharged electrode with the electrolytes and thereby could further facilitate the subsequent charging process.

4. CONCLUSIONS

In conclusion, we have synthesized different metallopolymer nanocomposites as O_2 electrodes for LOBs. The samples show interesting morphology as nanowalls grow vertically on the graphene surface, which is beneficial to achieve good performance as O_2 electrodes. The as-prepared Fe-based metallopolymer sample exhibits better round-trip efficiencies and cycling performance. It can repeatedly deliver discharge−charge capacities of 1000 mAh/g for 40 cycles and maintain round-trip efficiencies >78%. It also shows high first-cycle round-trip efficiencies of 79, 72, and 65% at current densities of 50, 200, and 400 mA/g, respectively.

■ ASSOCIATED CONTENT

Supporting Information

TEM image and XRD patterns of Fe-based metallopolymer/rGO, SEM images and electrochemical performance of Co-based metallopolymer/rGO and Mn-based metallopolymer/rGO, SEM images of the discharged electrodes and the schematic growth of the discharge products. This material is available free of charge via the Internet at http://pubs.acs.org.

■ AUTHOR INFORMATION

Corresponding Author

*E-mail: alexyan@ntu.edu.sg. Fax: +65 6790 9081. Tel: +65 6790 4583.

Notes

The authors declare no competing financial interest.

■ ACKNOWLEDGMENTS

We gratefully acknowledge Singapore MOE AcRF Tier 1 grants RG2/13, A*STAR SERC grant 1021700144, Singapore MPA

23/04.15.03 grant, and Singapore National Research Foundation under CREATE program: EMobility in Megacities.

REFERENCES

(1) Tarascon, J. M.; Armand, M. Issues and Challenges Facing Rechargeable Lithium Batteries. *Nature* **2001**, *414* (6861), 359−367.

(2) Bruce, P. G.; Freunberger, S. A.; Hardwick, L. J.; Tarascon, J.-M. Li-O_2 and Li-S Batteries with High Energy Storage. *Nat. Mater.* **2012**, *11* (1), 19−29.

(3) Cheng, F.; Chen, J. Metal-Air Batteries: from Oxygen Reduction Electrochemistry to Cathode Catalysts. *Chem. Soc. Rev.* **2012**, *41* (6), 2172−2192.

(4) Girishkumar, G.; McCloskey, B.; Luntz, A. C.; Swanson, S.; Wilcke, W. Lithium - Air Battery: Promise and Challenges. *J. Phys. Chem. Lett.* **2010**, *1* (14), 2193−2203.

(5) Ogasawara, T.; Débart, A.; Holzapfel, M.; Novák, P.; Bruce, P. G. Rechargeable Li_2O_2 Electrode for Lithium Batteries. *J. Am. Chem. Soc.* **2006**, *128* (4), 1390−1393.

(6) Freunberger, S. A.; Chen, Y. H.; Peng, Z. Q.; Griffin, J. M.; Hardwick, L. J.; Barde, F.; Novak, P.; Bruce, P. G. Reactions in the Rechargeable Lithium-O_2 Battery with Alkyl Carbonate Electrolytes. *J. Am. Chem. Soc.* **2011**, *133* (20), 8040−8047.

(7) Lu, Y. C.; Xu, Z. C.; Gasteiger, H. A.; Chen, S.; Hamad-Schifferli, K.; Shao-Horn, Y. Platinum-Gold Nanoparticles: A Highly Active Bifunctional Electrocatalyst for Rechargeable Lithium-Air Batteries. *J. Am. Chem. Soc.* **2010**, *132* (35), 12170−12171.

(8) Lu, Y.-C.; Gasteiger, H. A.; Shao-Horn, Y. Catalytic Activity Trends of Oxygen Reduction Reaction for Nonaqueous Li-Air Batteries. *J. Am. Chem. Soc.* **2011**, *133* (47), 19048−19051.

(9) Oh, S. H.; Black, R.; Pomerantseva, E.; Lee, J.-H.; Nazar, L. F. Synthesis of a Metallic Mesoporous Pyrochlore as a Catalyst for Lithium−O_2 Batteries. *Nat. Chem.* **2012**, *4* (12), 1004−1010.

(10) Black, R.; Oh, S. H.; Lee, J. H.; Yim, T.; Adams, B.; Nazar, L. F. Screening for Superoxide Reactivity in Li-O_2 Batteries: Effect on Li_2O_2/LiOH Crystallization. *J. Am. Chem. Soc.* **2012**, *134* (6), 2902−2905.

(11) Zhang, W.; Zhu, J.; Ang, H.; Zeng, Y.; Xiao, N.; Gao, Y.; Liu, W.; Hng, H. H.; Yan, Q. Binder-Free Graphene Foams for O_2 Electrodes of Li-O_2 Batteries. *Nanoscale* **2013**, *5*, 9651−9658.

(12) Zhang, W.; Zeng, Y.; Xu, C.; Tan, H.; Liu, W.; Zhu, J.; Xiao, N.; Hng, H. H.; Ma, J.; Hoster, H. E.; Yazami, R.; Yan, Q. Fe_2O_3 Nanocluster-Decorated Graphene as O_2 Electrode for High Energy Li-O_2 Batteries. *RSC Adv.* **2012**, *2* (22), 8508−8514.

(13) Chen, Y.; Freunberger, S. A.; Peng, Z.; Fontaine, O.; Bruce, P. G. Charging a Li−O_2 Battery Using a Redox Mediator. *Nat. Chem.* **2013**, *5* (6), 489−494.

(14) Shui, J.-L.; Okasinski, J. S.; Kenesei, P.; Dobbs, H. A.; Zhao, D.; Almer, J. D.; Liu, D.-J., Reversibility of Anodic Lithium in Rechargeable Lithium−Oxygen Batteries. *Nat. Commun.* **2013**, *4*.

(15) Peng, Z. Q.; Freunberger, S. A.; Chen, Y. H.; Bruce, P. G. A Reversible and Higher-Rate Li-O_2 Battery. *Science* **2012**, *337* (6094), 563−566.

(16) Shui, J.-L.; Karan, N. K.; Balasubramanian, M.; Li, S.-Y.; Liu, D.-J. Fe/N/C Composite in Li−O_2 Battery: Studies of Catalytic Structure and Activity toward Oxygen Evolution Reaction. *J. Am. Chem. Soc.* **2012**, *134* (40), 16654−16661.

(17) Jin, L.; Xu, L. P.; Morein, C.; Chen, C. H.; Lai, M.; Dharmarathna, S.; Dobley, A.; Suib, S. L. Titanium Containing Gamma-MnO_2 Hollow Spheres: One-Step Synthesis and Catalytic Activities in Li/Air Batteries and Oxidative Chemical Reactions. *Adv. Funct. Mater.* **2010**, *20* (19), 3373−3382.

(18) Xu, J.-J.; Xu, D.; Wang, Z.-L.; Wang, H.-G.; Zhang, L.-L.; Zhang, X.-B. Synthesis of Perovskite-Based Porous $La_{0.75}Sr_{0.25}MnO_3$ Nanotubes as a Highly Efficient Electrocatalyst for Rechargeable Lithium−Oxygen Batteries. *Angew. Chem., Int. Ed.* **2013**, *52* (14), 3887−3890.

(19) Lu, Y.-C.; Kwabi, D. G.; Yao, K. P. C.; Harding, J. R.; Zhou, J.; Zuin, L.; Shao-Horn, Y. The Discharge Rate Capability of Rechargeable Li-O_2 Batteries. *Energy Environ. Sci.* **2011**, *4* (8), 2999−3007.

(20) Wu, G.; More, K. L.; Johnston, C. M.; Zelenay, P. High-Performance Electrocatalysts for Oxygen Reduction Derived from Polyaniline, Iron, and Cobalt. *Science* **2011**, *332* (6028), 443−447.

(21) Wu, G.; Johnston, C. M.; Mack, N. H.; Artyushkova, K.; Ferrandon, M.; Nelson, M.; Lezama-Pacheco, J. S.; Conradson, S. D.; More, K. L.; Myers, D. J.; Zelenay, P. Synthesis-structure-performance Correlation for Polyaniline-Me-C non-precious Metal Cathode Catalysts for Oxygen Reduction in Fuel Cells. *J. Mater. Chem.* **2011**, *21* (30), 11392−11405.

(22) Bashyam, R.; Zelenay, P. A Class of Non-precious Metal Composite Catalysts for Fuel Cells. *Nature* **2006**, *443* (7107), 63−66.

(23) Li, Q.; Xu, P.; Gao, W.; Ma, S.; Zhang, G.; Cao, R.; Cho, J.; Wang, H.-L.; Wu, G. Graphene/Graphene-Tube Nanocomposites Templated from Cage-Containing Metal-Organic Frameworks for Oxygen Reduction in Li−O_2 Batteries. *Adv. Mater.* **2013**, 1378−1386.

(24) Zhu, Y. W.; Murali, S.; Stoller, M. D.; Ganesh, K. J.; Cai, W. W.; Ferreira, P. J.; Pirkle, A.; Wallace, R. M.; Cychosz, K. A.; Thommes, M.; Su, D.; Stach, E. A.; Ruoff, R. S. Carbon-Based Supercapacitors Produced by Activation of Graphene. *Science* **2011**, *332* (6037), 1537−1541.

(25) Li, X. L.; Wang, X. R.; Zhang, L.; Lee, S. W.; Dai, H. J. Chemically Derived Ultrasmooth Graphene Nanoribbon Semiconductors. *Science* **2008**, *319* (5867), 1229−1232.

(26) Novoselov, K. S.; Geim, A. K.; Morozov, S. V.; Jiang, D.; Zhang, Y.; Dubonos, S. V.; Grigorieva, I. V.; Firsov, A. A. Electric Field Effect in Atomically Thin Carbon Films. *Science* **2004**, *306* (5696), 666−669.

(27) Lin, C.-T.; Loan, P. T. K.; Chen, T.-Y.; Liu, K.-K.; Chen, C.-H.; Wei, K.-H.; Li, L.-J. Label-Free Electrical Detection of DNA Hybridization on Graphene using Hall Effect Measurements: Revisiting the Sensing Mechanism. *Adv. Funct. Mater.* **2013**, *23* (18), 2301−2307.

(28) Chai, N.-N.; Zeng, J.; Zhou, K.-G.; Xie, Y.-L.; Wang, H.-X.; Zhang, H.-L.; Xu, C.; Zhu, J.-X.; Yan, Q.-Y. Free-Radical-Promoted Conversion of Graphite Oxide into Chemically Modified Graphene. *Chem.—Eur. J.* **2013**, *19* (19), 5948−5954.

(29) Yang, X.; Cheng, C.; Wang, Y.; Qiu, L.; Li, D. Liquid-Mediated Dense Integration of Graphene Materials for Compact Capacitive Energy Storage. *Science* **2013**, *341* (6145), 534−537.

(30) Yang, K.; Hu, L.; Ma, X.; Ye, S.; Cheng, L.; Shi, X.; Li, C.; Li, Y.; Liu, Z. Multimodal Imaging Guided Photothermal Therapy using Functionalized Graphene Nanosheets Anchored with Magnetic Nanoparticles. *Adv. Mater.* **2012**, *24* (14), 1868−1872.

(31) Laoire, C. O.; Mukerjee, S.; Abraham, K. M.; Plichta, E. J.; Hendrickson, M. A. Elucidating the Mechanism of Oxygen Reduction for Lithium-Air Battery Applications. *J. Phys. Chem. C* **2009**, *113* (46), 20127−20134.

(32) Guo, Z.; Zhou, D.; Dong, X.; Qiu, Z.; Wang, Y.; Xia, Y. Ordered Hierarchical Mesoporous/Macroporous Carbon: A High Performance Catalyst for Rechargeable Li−O_2 batteries. *Adv. Mater.* **2013**, 5668−5672.

(33) Hummers, W. S.; Offeman, R. E. Preparation of Graphitic Oxide. *J. Am. Chem. Soc.* **1958**, *80* (6), 1339−1339.

(34) Xu, Y.; Bai, H.; Lu, G.; Li, C.; Shi, G. Flexible Graphene Films via the Filtration of Water-Soluble Noncovalent Functionalized Graphene Sheets. *J. Am. Chem. Soc.* **2008**, *130* (18), 5856−5857.

(35) Zhu, J. X.; Zhu, T.; Zhou, X. Z.; Zhang, Y. Y.; Lou, X. W.; Chen, X. D.; Zhang, H.; Hng, H. H.; Yan, Q. Y. Facile Synthesis of Metal Oxide/Reduced Graphene Oxide Hybrids with High Lithium Storage Capacity and Stable Cyclability. *Nanoscale* **2011**, *3* (3), 1084−1089.

(36) Zhu, J.; Sun, K.; Sim, D.; Xu, C.; Zhang, H.; Hng, H. H.; Yan, Q. Nanohybridization of Ferrocene Clusters and Reduced Graphene Oxides with Enhanced Lithium Storage Capability. *Chem. Commun.* **2011**, *47* (37), 10383−10385.

(37) Su, C. Y.; Lu, A. Y.; Xu, Y. P.; Chen, F. R.; Khlobystov, A. N.; Li, L. J. High-Quality Thin Graphene Films from Fast Electrochemical Exfoliation. *ACS Nano* **2011**, *5* (3), 2332−2339.

(38) Zhang, X.; Xu, j.-J.; Wang, Z.; Xu, D.; Wang, H. 3D Ordered Macroporous $LaFeO_3$ as Efficient Electrocatalyst for Li-O_2 Batteries

with Enhanced Rate Capability and Cyclic Performance. *Energy Environ. Sci.* **2013**.
(39) Wu, G.; Mack, N. H.; Gao, W.; Ma, S.; Zhong, R.; Han, J.; Baldwin, J. K.; Zelenay, P. Nitrogen-Doped Graphene-Rich Catalysts Derived from Heteroatom Polymers for Oxygen Reduction in Nonaqueous Lithium−O_2 Battery Cathodes. *ACS Nano* **2012**, *6* (11), 9764−9776.
(40) Jian, Z.; Liu, P.; Li, F.; He, P.; Guo, X.; Chen, M.; Zhou, H. Core−Shell-Structured CNT@RuO2 Composite as a High-Performance Cathode Catalyst for Rechargeable Li−O_2 Batteries. *Angew. Chem. Int. Ed.* **2013**, *2* (53), 442−446.
(41) Zhang, L.; Zhang, S.; Zhang, K.; Xu, G.; He, X.; Dong, S.; Liu, Z.; Huang, C.; Gu, L.; Cui, G. Mesoporous $NiCo_2O_4$ Nanoflakes as Electrocatalysts for Rechargeable Li-O_2 Batteries. *Chem. Commun.* **2013**, *49* (34), 3540−3542.
(42) Wang, L.; Zhao, X.; Lu, Y. H.; Xu, M. W.; Zhang, D. W.; Ruoff, R. S.; Stevenson, K. J.; Goodenough, J. B. $CoMn_2O_4$ Spinel Nanoparticles Grown on Graphene as Bifunctional Catalyst for Lithium-Air Batteries. *J. Electrochem. Soc.* **2011**, *158* (12), A1379−A1382.
(43) Ottakam Thotiyl, M. M.; Freunberger, S. A.; Peng, Z.; Bruce, P. G. The Carbon Electrode in Nonaqueous Li−O_2 Cells. *J. Am. Chem. Soc.* **2012**, *135*, 494−450.
(44) Sharon, D.; Etacheri, V.; Garsuch, A.; Afri, M.; Frimer, A. A.; Aurbach, D. On the Challenge of Electrolyte Solutions for Li−Air Batteries: Monitoring Oxygen Reduction and Related Reactions in Polyether Solutions by Spectroscopy and EQCM. *J. Phys. Chem. Lett.* **2012**, *4* (1), 127−131.